Multimodality Imaging of Anatomy and Function in Coronary Artery Disease

Schuijf, J.D.

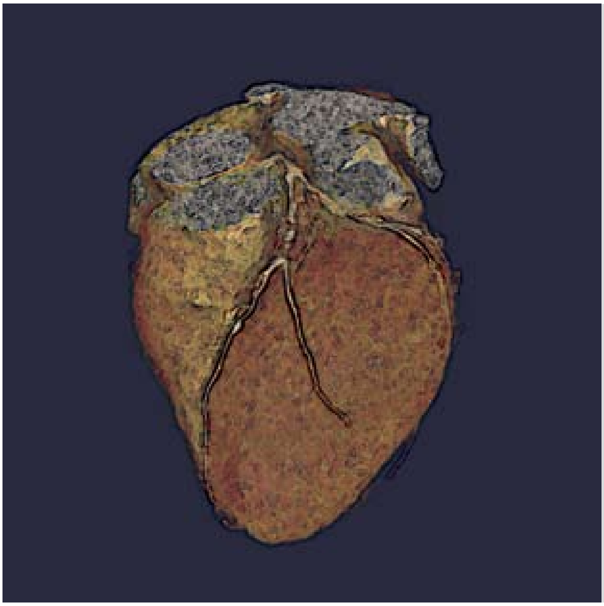

Part I

Non-Invasive Coronary Angiography with Multi-Slice Computed Tomography; Introduction and Diagnostic Accuracy

Chapter 2

Multi-Slice CT Coronary Angiography: How to do it and What is the Current Clinical Performance?

Filippo Cademartiri, Joanne D. Schuijf, Nico R. Mollet, Patrizia Malagutti, Giuseppe Runza, Jeroen J. Bax, Pim J. de Feyter

Eur J Nucl Med Mol Imaging 2005; 32: 1337-1347

Abstract

The introduction of multi-slice computed tomography (MSCT) has allowed non-invasive coronary angiography. Although widely applied, extensive information on technical details of the technique is lacking. In this manuscript, detailed information is provided on patient preparation, data acquisition, reconstruction and interpretation is provided. In addition, a summary on the available studies using MSCT for non-invasive angiography is provided. Based on pooled analysis of direct comparisons between MSCT and invasive angiography, the weighted mean sensitivity and specificity of current 16-slice MSCT to detect coronary artery disease are 88% and 96% respectively. At present, the technique is particularly well-suited to reliably exclude coronary artery disease. It is important to emphasize that MSCT only provides anatomical images, visualizing the presence of atherosclerosis, but information on the hemodynamic significance of these lesions (i.e. ischemia) can not be derived.

Introduction

Multi-slice computed tomography (MSCT) has attracted a lot of attention recently. This technique allows non-invasive visualization of the coronary arteries and comparison with invasive coronary angiography has yielded good results [1-3]. In particular, many studies have recently been published on the accuracy of MSCT to detect (or exclude) coronary artery disease. Currently, comprehensive information on the technique and its clinical value is lacking. In this manuscript, a summary is provided on the data acquisition, reconstruction and analysis with MSCT; also, a summary on the accuracy of the technique to assess coronary artery disease, based on the available studies, is provided.

How to perform MSCT, data acquisition

Various issues are of importance in data acquisition with MSCT. High heart rates influence image quality and patients with heart rates ≥65 bpm should receive beta-blockers orally before the scan, unless contra-indicated. Patients with (supra-)ventricular arrhythmias should not undergo MSCT unless software that allows the editing of the ECG is available (see below) [4].
The contrast agent should be administered through an antecubital vein to allow high flow rates [5]. High intravascular attenuation and low beam-hardening artefacts in the right heart are recommended for an optimal MSCT coronary angiogram (CA). On average a bolus of 100 ml of iodine contrast material (350-400 mgl/ml) administered at 3-5 ml/s, immediately followed by 40 ml saline, provides optimal arterial enhancement [6;7]. To synchronize the arrival of contrast material in the coronary arteries and the scan, a test bolus or bolus tracking can be used [5;8].
The optimal scan protocol results in high spatial resolution (thinner collimation), a high temporal resolution (faster gantry rotation) with low radiation exposure (prospectively ECG-triggered tube current modulation [9]) compatible with a good signal to noise ratio (Figure 1).

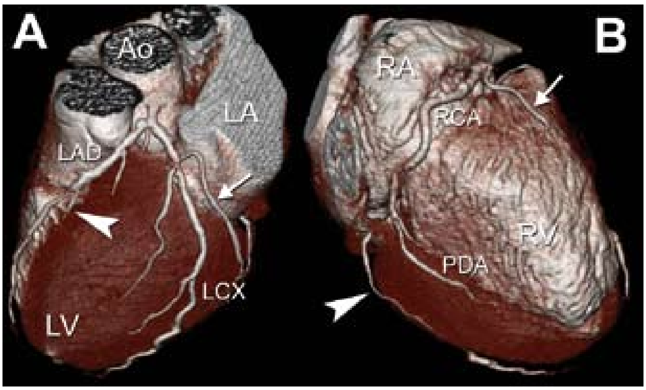

Abbreviations: Ao= ascending aorta; LA= left atrium; LV= left ventricle; LAD= left anterior descending; LCX= left circumflex; RA= right atrium; RV= right ventricle; RCA= right coronary artery; PDA= posterior descending artery.

Figure 1. Three-dimensional volume rendering using 64-slice MSCT. Small diagonal branches of the LAD (Panel A, arrowhead), the obtuse marginal branches of the LCX (Panels A, arrow and B, arrowhead), the acute marginal branches of the RCA (Panel B, arrow), and the PDA are clearly visible.

How to perform MSCT, data reconstruction

Since the ECG is simultaneously registered during the examination, the acquired raw data can be reconstructed at any time point during the cardiac cycle. When performing these reconstructions, several approaches can be used, which are depicted in Figure 2 [10;11]. During the most widely used approach, data are reconstructed at a fixed percentage delay based on the R wave. However, data can also be reconstructed using an absolute prospective delay based on the previous R wave, although this technique is more sensitive to minimal variations in heart rate and therefore may result in data inconsistencies. The third approach, which is also frequently applied, utilizes an absolute reverse delay based on the upcoming R wave. As a result, data are reconstructed during end-diastole regardless of the absolute heart rate or potential variations in heart rate. Finally, the temporal window can theoretically also be positioned on the top of the P wave. Although this approach allows accurate reconstruction of data in end-diastole, it is not commonly performed due to the current unavailability of software that recognizes P waves.

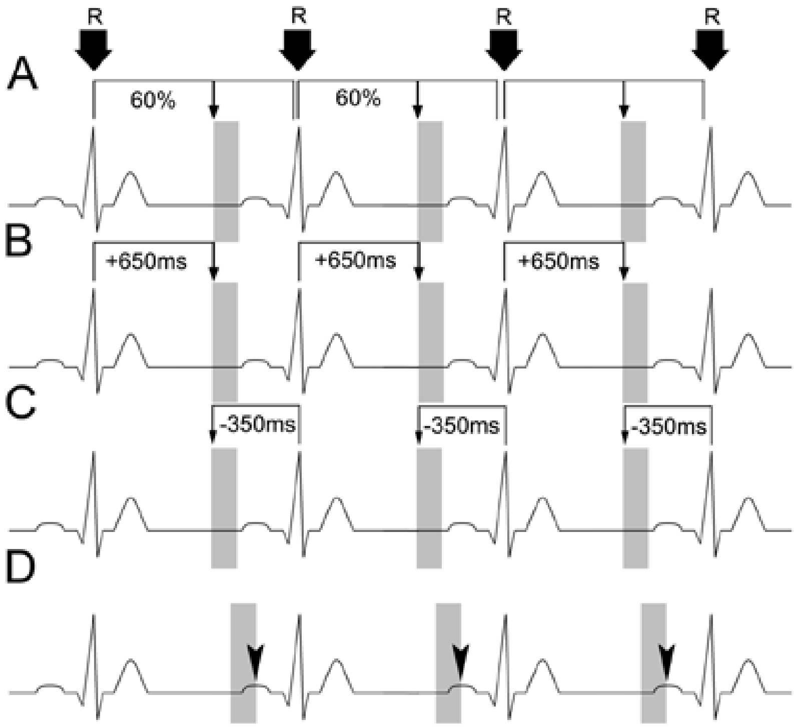

Figure 2. Retrospective reconstruction of MSCT image data sets. Several different methods are available to define the temporal window in which the image data set is reconstructed. In Panel A, data are reconstructed using a fixed percentage delay, in this case at every 60% of the cardiac interval. In Panel B, an absolute prospective delay is used, resulting in the reconstruction of images at 650 ms after every R-peak. The same temporal window is achieved in Panel C however, by reconstructing at an absolute reverse delay, which is in this case 350 ms before every R-peak. In Panel D, the temporal window for data reconstruction is set with its end on the top of the P wave in order to allow reconstruction of images during the very last moment of limited cardiac motion before systolic contraction.

At present, no consensus has been established concerning which protocol provides the most optimal results, and frequently a mixture of the available approaches is used. The phase of the cardiac cycle providing most of the information is the mid-to-end diastole, when the heart is in the iso-volumetric filling phase and motion is minimal. In some cases, including patients with higher heart rates during data acquisition, the tele-systolic phase can also provide relevant information since at the end of myocardial contraction, the motion of the coronary arteries is also reduced (Figure 3).

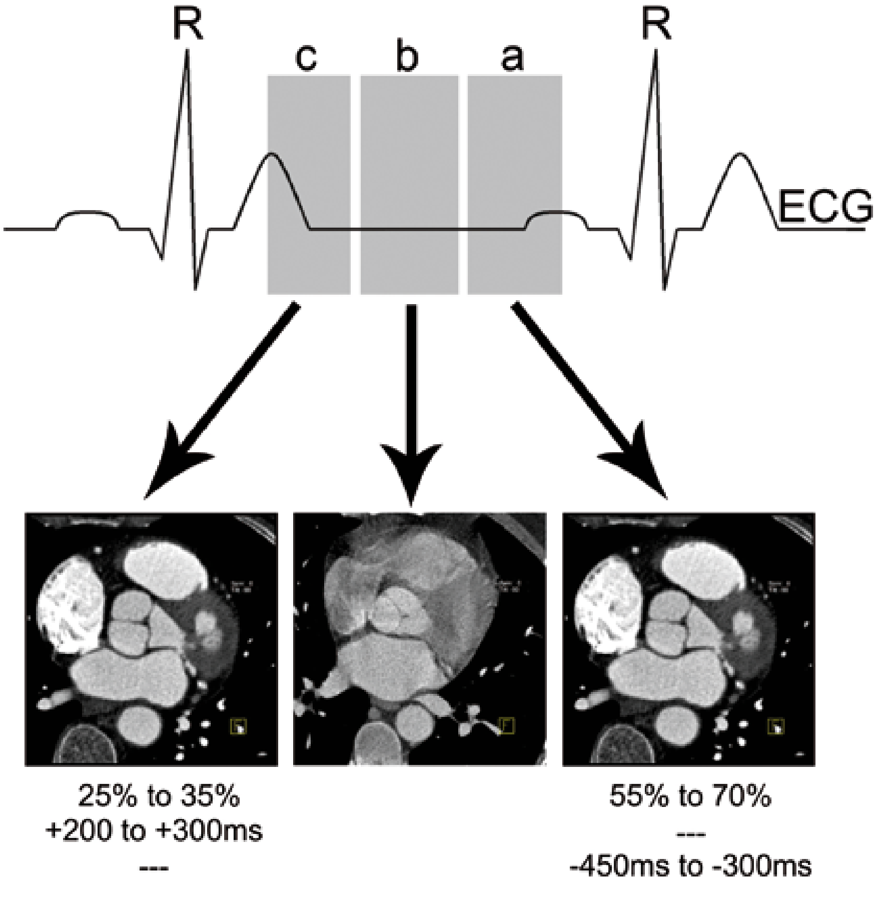

Figure 3. The position of the temporal reconstruction window. Three main areas in the cardiac cycle are relevant for MSCT image reconstruction. The tele-diastolic phase (a), which typically occurs at 55% to 70% of the R-R interval, represents the cardiac phase without contraction and thus minimal motion. During the tele-systolic phase (c, typically 25% to 40% of the R-R interval) isovolumetric contraction occurs, resulting in reduced coronary motion as well. In between lies the early-to-mid diastolic phase (b) during which some residual motion is present.

An important feature of some ECG-gating software is the possibility to edit the position of the temporal windows within the cardiac cycle, and to exclude ECG irregularities such as pre-mature ventricular beats (or extra-systoles) (Figure 4) [4]. Another relevant reconstruction parameter is the effective slice width that is usually slightly thicker than the minimal collimation in order to improve the signal to noise ratio. The reconstruction increment should be around 50% of the effective slice thickness to improve the spatial resolution and the oversampling along the z-axis. The field of view should be as small as possible including the entire heart in order to fully exploit the constant image matrix (512 x 512 pixels). The filtering should be a trade-off between the noise and the quality of the image. Usually medium convolution filters are applied for coronary imaging. Higher filters improve visualization of calcified vessel walls or stent struts and the lumen within the stents (Figure 5).

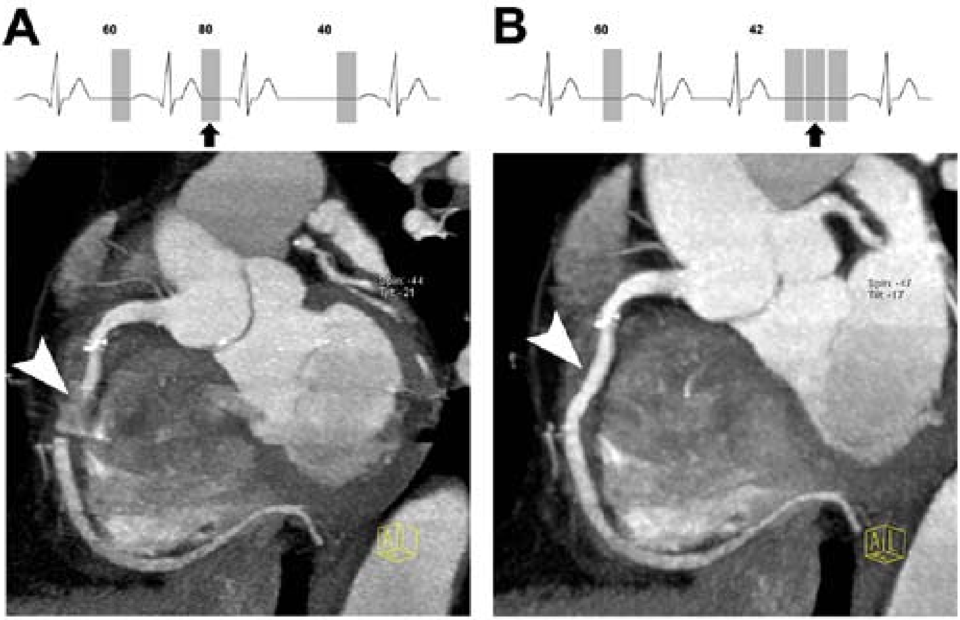

Figure 4. Editing of the ECG in the presence of premature ventricular beats.
The presence of a premature beat can result in motion artifacts on MSCT. The explanation for this is related to the mis-alignment of the temporal window in the diastolic pause before the premature beat (Panel A, arrow in ECG tracing). This results in motion artifacts that worsen the image quality (Panel A, arrowhead). The operator should delete the temporal window during the premature beat and fill the following long diastolic pause with additional temporal windows (Panel B, arrow in the ECG tracing) until the minimum heart rate interval is achieved. Accordingly, recovery of data is possible and diagnostic image quality can be obtained (Panel B, arrowhead).

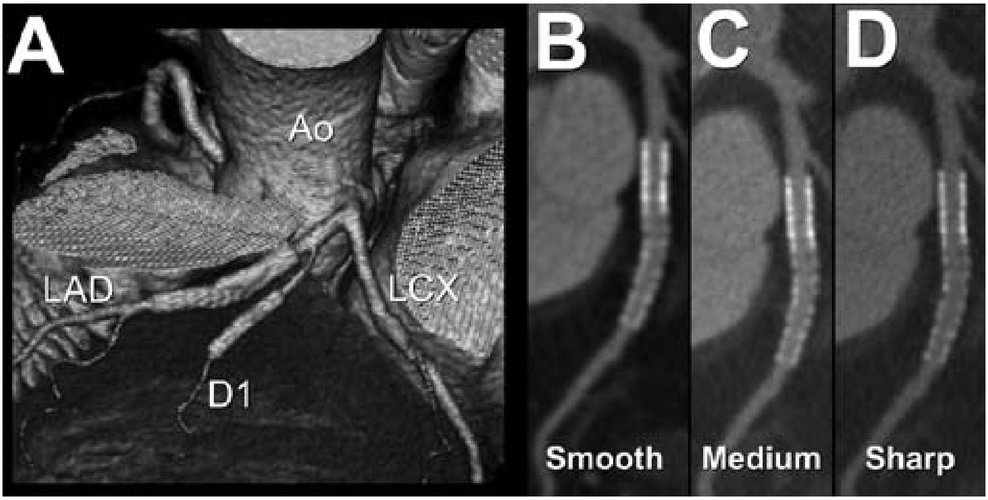

Figure 5. Effect of convolution filters on stent visualization. In Panel A, the 3D volume rendered image shows a left coronary artery with two stents in the LAD and in the first diagonal branch (D1). The stent in the LAD is displayed in curved multiplanar reconstructions in panels B, C, and D using progressively sharper convolution filters. The visualization of the stents and the differentiation between the struts and the lumen is improved by sharp convolution filters.
Abbreviations: Ao= ascending aorta; LAD= left anterior descending; LCX= left circumflex.

How to perform MSCT, data interpretation

To date, the studies reported have used semi-quantitative detection of significant stenosis (defined as ≥50% lumen reduction) [12-14], no studies with quantitative MSCT-CA have been reported yet. The coronary arteries are evaluated according to scoring systems used for invasive CA and include a 15- or 16-segment model suggested by the American Heart Association [15] (Figure 6). Axial images should always be reviewed first, in order to detect possible morphological abnormalities or non-coronary findings e.g. pulmonary nodules.

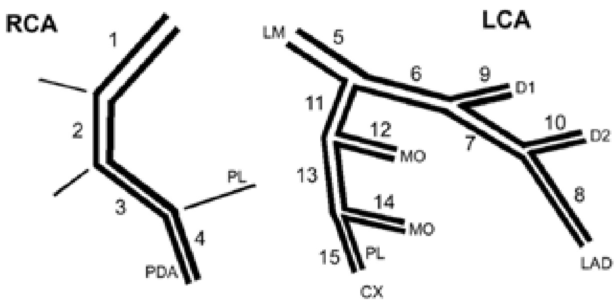

Figure 6. Classification of coronary segments can be performed by dividing the coronary tree into 15 segments (modified from the American Heart Association [15]). This classification includes most of the segments with a diameter larger than 1.5 mm.
Abbreviations: LCA= left coronary artery; CX= left circumflex; LAD= left anterior descending; LM= left main; MO= marginal branch; RCA= right coronary artery; D1= first diagonal branch; D2= second diagonal branch; PL= postero-lateral branch; PDA= posterior descending artery.

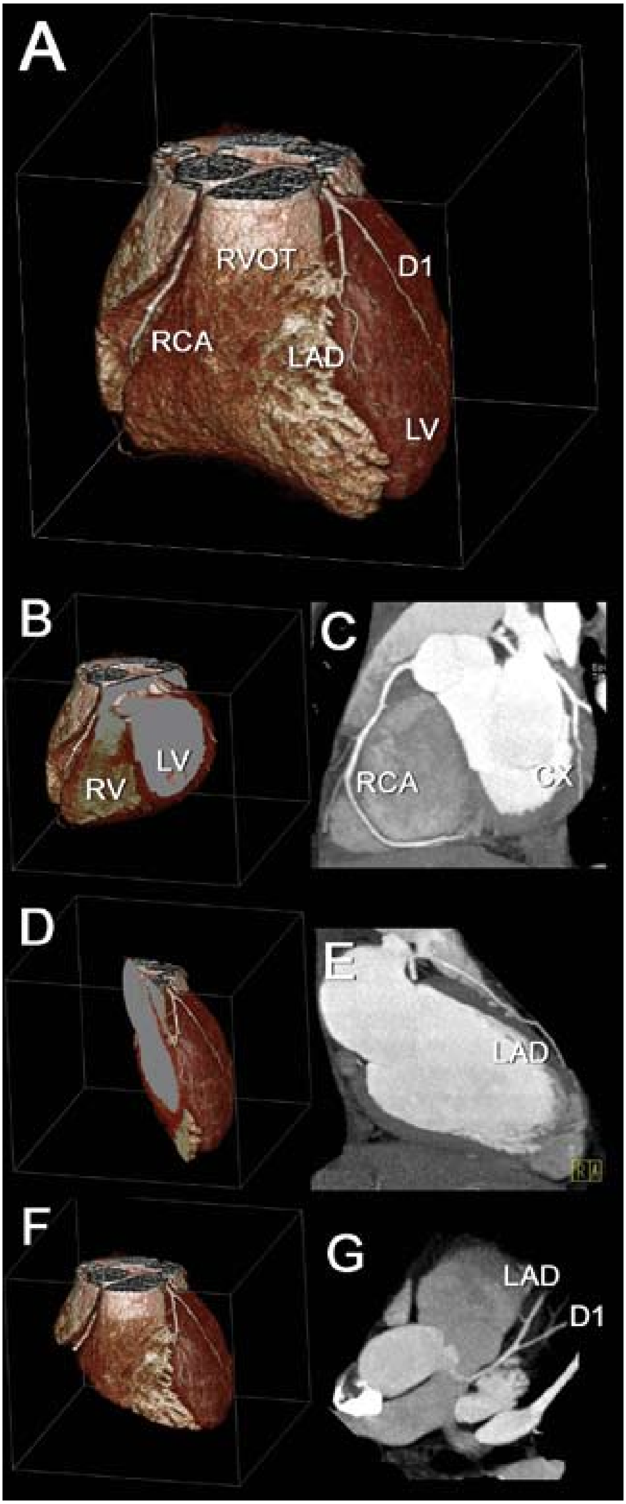

Figure 7. Planes adopted on MSCT for the visualization of coronary arteries. Using the 3D volume rendered image as a reference (Panel A) the three main planes for visualization of the coronary arteries are displayed. The atrio-ventricular plane with volume rendering (Panel B) and the corresponding cross-section with maximum intensity projection (Panel C) allow visualization of the RCA and CX. The inter-ventricular plane (Panels D and E) allows the visualization of the LAD along the anterior wall of the left ventricle. The para-axial plane parallel to the LAD (Panels F and G) allows the visualization of the LAD and the diagonal branches.
Abbreviations: CX= left circumflex; D1= first diagonal branch; LAD= left anterior descending coronary artery; LV= left ventricle; RCA= right coronary artery; RV= right ventricle; RVOT= right ventricle outflow tract.

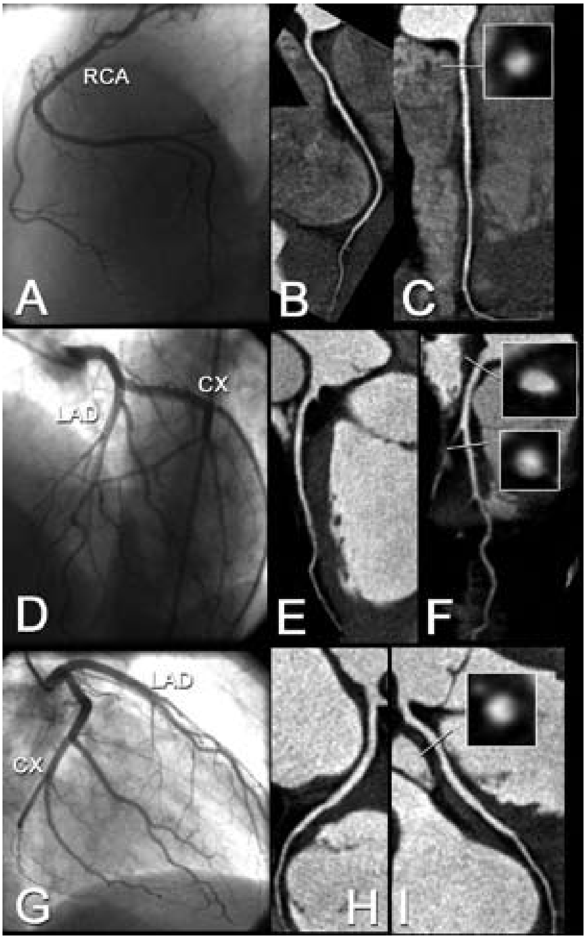

Figure 8. Curved central-lumen-line reconstructions on MSCT. The conventional coronary angiogram and the curved reconstructions are displayed for the RCA (Panels A-C), the LAD (Panels D-F), and for the CX (Panels G-I). For each vessel an orthogonal cross section performed in a region close to the ostium is displayed. *Abbreviations: CX= left circumflex; LAD= left anterior descending coronary artery; RCA= right coronary artery.*

The multiplanar reconstructions (MPR) are employed for the evaluation of coronary arteries. The main planes useful are: 1) plane parallel to the atrio-ventricular groove (allows the longitudinal visualization of the right coronary artery and of the left circumflex coronary artery) 2) plane parallel to the inter-ventricular groove (allows visualization of the left anterior descending coronary artery) (see Figures 7 and 8).

On these planes a maximum intensity projection algorithm can be useful (from 5-8 mm to 3 mm of thickness, depending on extent and severity of calcifications). When the vessel is displayed within one plane, dedicated software permits to perform a central-lumen line reconstruction and the resulting image can be rotated 360° around its axis (Figure 8).

In parallel, an orthogonal view of the same vessel is displayed, allowing a better evaluation of stenosis. In general, 3D volume rendering is performed to provide an overview (and variations) of the coronary anatomy (total occlusions, aberrant coronary arteries) and should not be used for assessment of stenotic lesions (Figure 7).

Artifacts

Artifacts are mainly related to 8 issues (Table 1). Motion is commonly observed in MSCT-CA, and is mainly caused by (supra-)ventricular arrhythmias or breathing. Image noise can be related to obesity or to insufficient vascular contrast enhancement. Beam hardening is usually associated with high-attenuation objects such as surgical clips, stents and severe calcifications. Volume averaging is due to contamination by attenuation of high-attenuation objects surrounded by tissue with lower attenuation. Incorrect positioning of the temporal window can generate artifacts because there are only a few moments during the cardiac cycle when the heart stands still for a reasonable amount of milliseconds. Data can be missing because of irregularities in heart rate. Poor vascular enhancement is a result of low injection rate, low contrast volume, or iodine concentration. Images can be blurred because of several of the aforementioned issues.

Table 1. Classification and cause of artifacts.

Artifact	Description	Cause
Motion	High or irregular heart rate	Insufficient temporal resolution (Supra-)ventricular arrhythmias
	Patient breathing	
Image contrast/noise	Insufficient vascular enhancement	Inadequate contrast administration
	Obesity	High tissue absorption throughout the dataset
Beam hardening	Streak artifacts	Extensive calcifications, coronary artery stents, arterial clips
Volume averaging	"Blooming"	Extensive calcifications, coronary artery stents, arterial clips
Temporal window	Motion artifacts (HR independent)	Sub-optimal selection of temporal window
		Premature heart beats
		Irregular ECG-wave
Missing data	Lack of information	Irregular ECG baseline
		Mis-triggering
Vessel enhancement	Poor enhancement	Low injection rate, low volume, low iodine content
Image quality	Blurred images	See Motion
	Blurred vessels	See Vessel enhancement

Accuracy to assess coronary artery disease

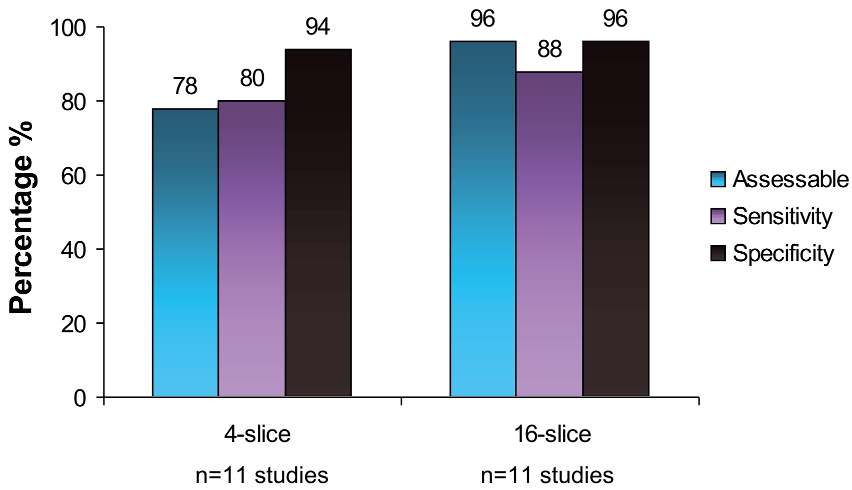

Figure 9. Bar graph showing the diagnostic accuracy of 4- and 16-slice MSCT for the evaluation of significant coronary artery stenoses (data based on reference [16]).
Assessable = the average percentage of coronary segments that were of sufficient image quality to include in the analyses concerning diagnostic accuracy.

During the past few years, extensive research has been invested in the development of non-invasive CA with MSCT, resulting in a considerable number of publications on the diagnostic accuracy of this technique. In 1998, the first generation of multi-slice scanners was introduced, allowing the simultaneous acquisition of 4 slices, thereby enabling MSCT systems to visualize the coronary arteries. Reported sensitivities and specificities ranged from 66% to 99%, with weighted means of respectively 80% and 94% [16]. To obtain these results however, more than 20% of the available segments were on average excluded, representing an important limitation of the technique at that stage.
More recently, results of the newer generation of 16-slice systems have become available. With these systems, sections as thin as 0.5 mm and a temporal resolution of 105-250 ms can be obtained. As a result, a considerable improvement in assessability (approximately 96%) as well as sensitivity (approximately 88%) could be observed, with no loss in specificity, as shown in Figure 9 [16]. Further refinement is anticipated by the introduction of 64-slice scanners that have been recently introduced, although currently no studies are available regarding the diagnostic accuracy of these systems. Examples of 64-slice MSCT-CA in patients with respectively normal and abnormal coronary arteries are provided in Figures 10 and 11.

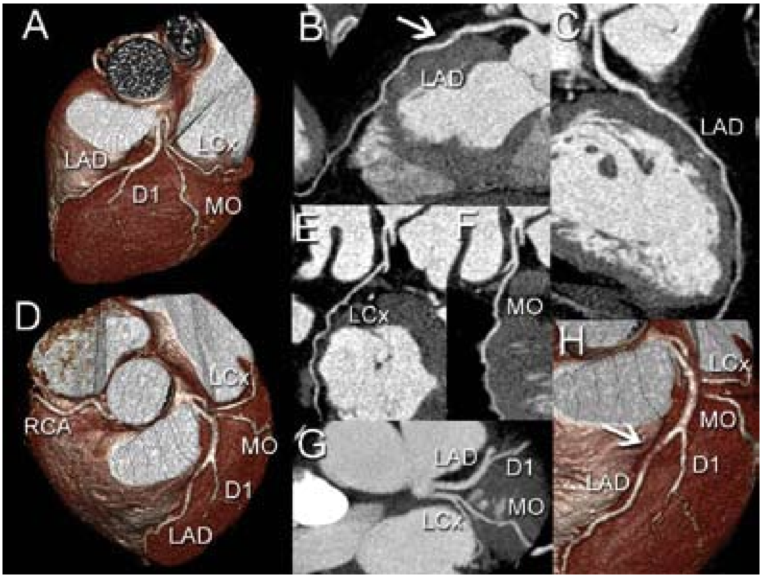

Figure 10. An example of normal coronary arteries obtained with 64-slice MSCT. An intra-myocardial course of the LAD can be observed (Panels B and H-arrows).
Abbreviations: LAD= left anterior descending coronary artery; D1= first diagonal branch; LCx= left circumflex coronary artery; MO= marginal branch.

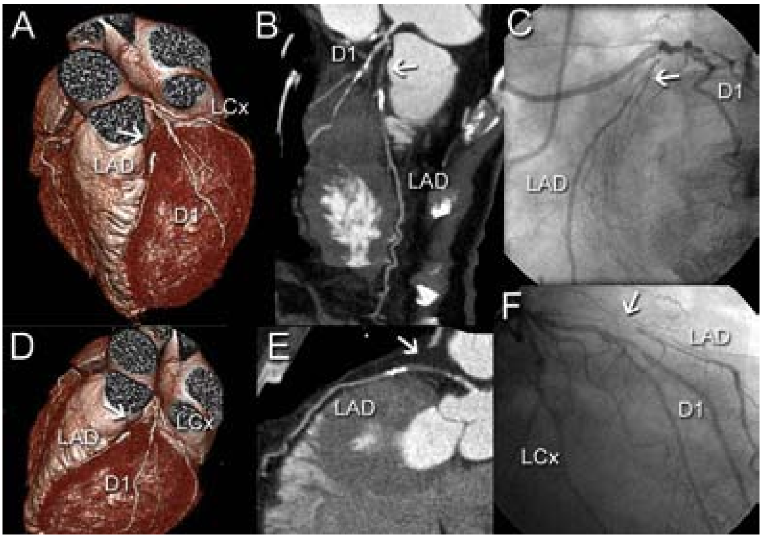

Figure 11. An example of a patient with a total occlusion of the LAD, obtained with 64-slice MSCT. The LAD is occluded (Panels A, B, D, E, arrows), whereas the first diagonal branch and the LCx are diffusely diseased. Conventional coronary angiography showed comparable findings (Panels C and F).
Abbreviations: LAD= left anterior descending coronary artery; D1= first diagonal branch; LCx= left circumflex coronary artery.

In patients presenting with recurrent angina after surgical or percutaneous revascularization, MSCT may be applied to assess patency of either coronary bypass grafts or stents. The axial course, large diameter and relative immobility of coronary bypass grafts during the cardiac cycle facilitate evaluation with MSCT. In Figure 12, an example is provided of 64-slice MSCT imaging of a patient with previous coronary bypass grafting. Several studies have explored the accuracy of MSCT to evaluate graft patency in comparison to conventional CA. In these 7 studies, with a total of 257 patients included, virtually all grafts were of sufficient image quality to assess patency [17-22]. Pooled analysis of these studies showed a weighted mean sensitivity of MSCT to detect graft occlusion of 88%, while the weighted mean specificity was 98%. In 5 studies, assessment of graft stenosis was undertaken [18-20;23;24]. In these studies, with 267 patients included, 80% of grafts were eligible for evaluation, with a weighted mean sensitivity and specificity of 84% and 95%, respectively. Data are summarized in Figure 13. Despite these encouraging results, still several important limitations remain. Metal artefacts resulting from surgical clips frequently obscure assessment, while difficulties are also encountered frequently in the evaluation of distal anastomoses and distal parts of sequential grafts.

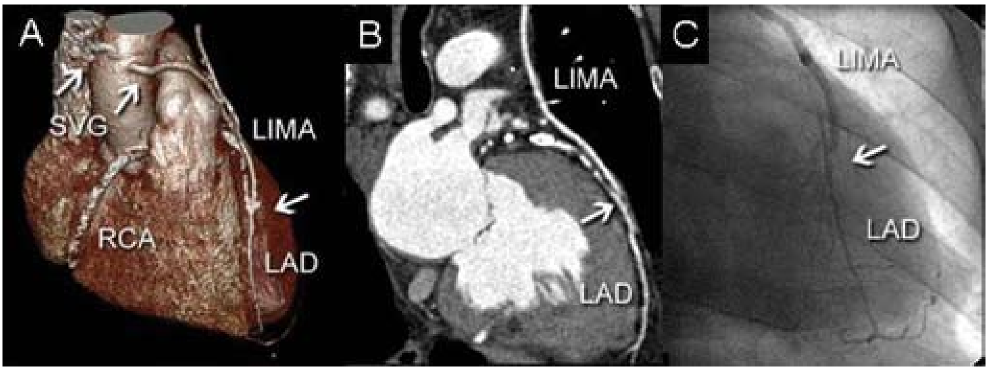

Figure 12. An example of a patient with previous coronary bypass surgery, obtained with 64-slice MSCT. As shown in Panels A and B, the LIMA is patent, while one of the 2 saphenous vein grafts is occluded (Panel A, left arrow). Conventional coronary angiography confirmed patency of the left internal mammary artery graft (Panel C).
Abbreviations: LAD= left anterior descending coronary artery; SVG= saphenous vein graft; LIMA= left internal mammary artery; RCA= right coronary artery.

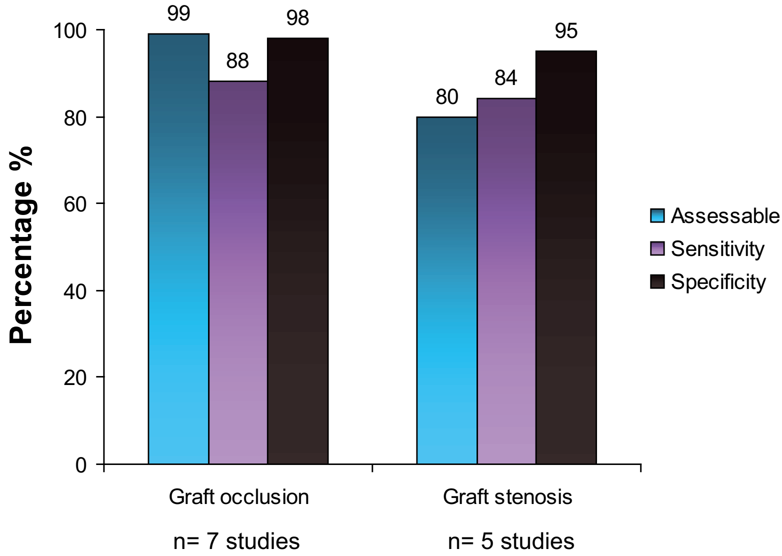

Figure 13. Bar graph showing the diagnostic accuracy of MSCT in the evaluation of patients after coronary bypass surgery (data based on references [17-24]).
Assessable = the average percentage of bypass grafts that were of sufficient image quality to include in the analyses concerning diagnostic accuracy.

Another application of MSCT that is currently under investigation is the assessment of coronary stents, which are difficult to image with MSCT. Their metal content leads to high-density artifacts, and subsequent obscuring of a considerable part of the stent lumen. In many studies regarding the diagnostic accuracy of MSCT therefore, stented segments are still excluded from analysis. However, substantial progress has been obtained with the increased image quality of the newer generation of MSCT scanners. With 4-slice systems, the stent lumen was virtually invisible, whereas with 16-slice systems improved visualization has been reported, in particular in stents with either a large diameter or thinner struts [25]. With the recently introduced 64-slice systems (Figure 14) as well as the previously discussed dedicated filters (Figure 5), an even higher percentage of stents will be eligible for assessment of patency. Still, artificial narrowing of the stent lumen will currently remain to some extent, thereby hampering detection of subtle neo-intima hyperplasia.

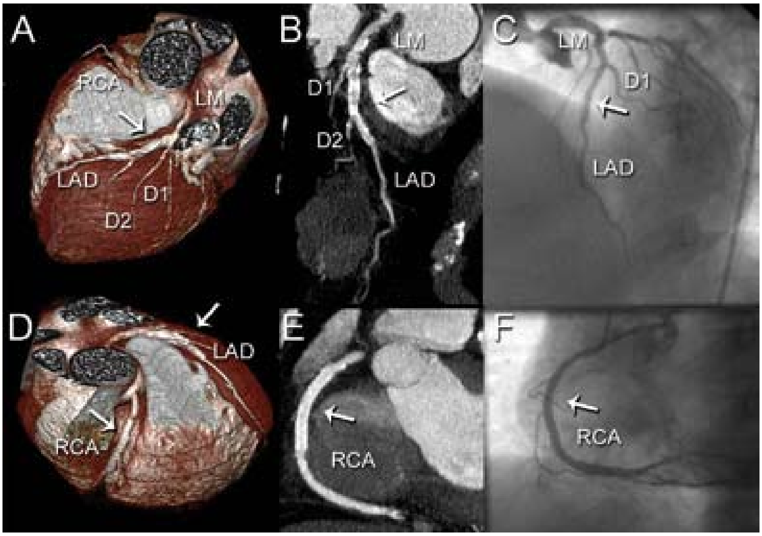

Figure 14. Coronary stent imaging with 64-slice MSCT. In Panels A and B, the patency of the stented LAD is demonstrated. In Panels D and E, absence of in-stent restenosis in the stented RCA is demonstrated. The MSCT findings were confirmed by conventional coronary angiography (Panels C and F).
Abbreviations: LAD= left anterior descending coronary artery; D1= first diagonal branch; D2= second diagonal branch; RCA= right coronary artery; LM= left main.

Additional applications of MSCT

Besides the assessment of coronary artery disease, MSCT can also be used for evaluation of left ventricular (LV) function; LV function (and LV volumes) are important prognostic parameters. Since MSCT data are acquired throughout the entire cardiac cycle, during continuous registration of the ECG, images can be reconstructed at any cardiac phase. As a result, information on LV function can be derived from the same data set as used for the evaluation of the coronary arteries.
In the assessment of LV ejection fraction, initial studies have shown good correlations between MSCT and either MRI or echocardiography [26-30]. In addition to global function, regional contractile function can be assessed (Figure 15). A recent comparison between MSCT and 2D echocardiography revealed an overall agreement of 91% in 493 segments evaluated for the presence of regional wall motion abnormalities [31]. Preferably, systolic wall thickening should be assessed during stress as well as resting conditions. However, with regard to the radiation dose associated with MSCT, such a protocol remains at present unattractive.

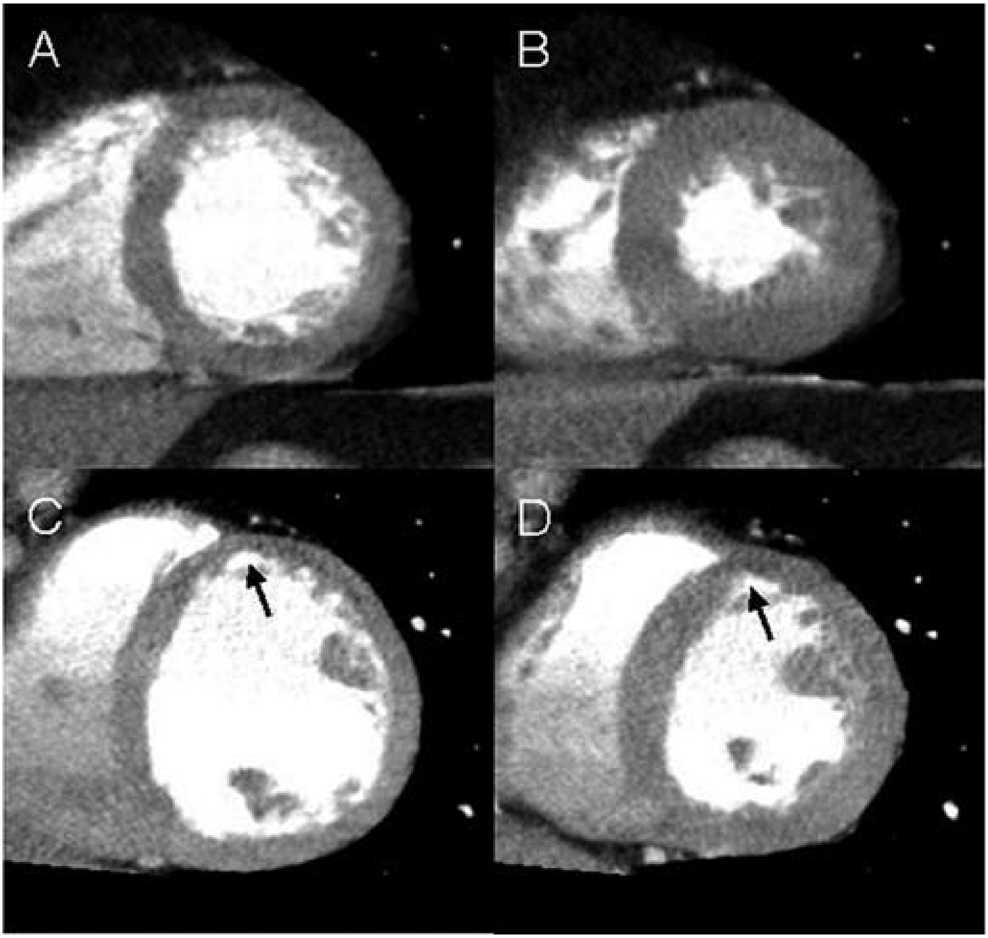

Figure 15. Regional wall motion analysis with 64-slice MSCT. In Panels A and B, short-axis left ventricular reconstructions in respectively end-diastole and end-systole are shown of a patient with normal wall motion; the left ventricular ejection fraction was 55%. In Panels C and D, similar reconstructions are shown of a patient with a previous anterior myocardial infarction. In the corresponding region (arrows), abnormal wall motion can be appreciated; the ventricular ejection fraction was 38%.

In addition to LV function, MSCT has been used for the evaluation of pulmonary vein anatomy in patients with atrial fibrillation considered for pulmonary vein ablation. Ectopic foci located within the pulmonary veins have been linked to the induction of atrial fibrillation and/or tachycardia [32]. As a result, different percutaneous ablation strategies have been developed to either eliminate the pulmonary venous foci or encircle and electrically isolate the pulmonary veins from the left atrium. Despite a good success rate of these strategies, the procedure and fluoroscopy times are still considerable due to several reasons. The veno-atrial junctions and the pulmonary veins or their ostia are not easily visualized using fluoroscopy, while the pulmonary venous anatomy itself is highly variable [33]. Knowledge of pulmonary venous anatomy, including potential anomalies in number and insertion of pulmonary veins as well as ostial shape, prior to the ablation procedure, therefore, would be of great benefit and potentially facilitate procedures. Preliminary studies have demonstrated that this information can be provided by MSCT [34]. In Figure 16, an example of visualization of different variants of pulmonary vein anatomy by MSCT is provided. Jongbloed et al recently performed a head-to-head comparison between MSCT and intracardiac echocardiography in 42 patients prior to pulmonary vein ablation [35]. The authors observed a higher sensitivity for MSCT in the detection of additional branches and right-sided early branching. In addition, an underestimation of ostial size by intracardiac echocardiography was demonstrated. These findings underline the superiority of 3D imaging techniques to demonstrate asymmetrical shape of pulmonary vein ostia. Further investigations however are needed to evaluate how MSCT data can be used or integrated with other data for optimization of pulmonary vein ablation strategies.

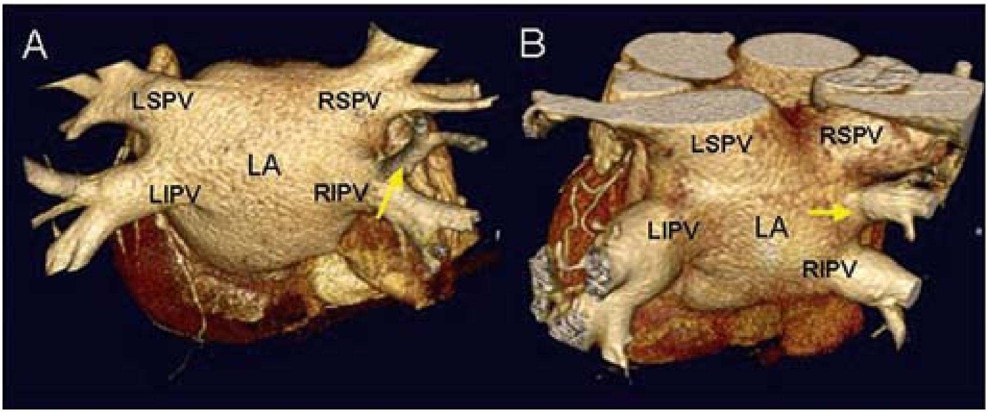

Figure 16. Different variants of pulmonary vein anatomy, as visualized by 3D volume rendered 64-slice MSCT reconstructions. In Panel A, early branching (arrow) of the right inferior pulmonary vein can be observed. An additional right pulmonary vein can be observed in Panel B (arrow).
Abbreviations: LA= left atrium; LIPV= left inferior pulmonary vein; LSPV= left superior pulmonary vein; RIPV= right inferior pulmonary vein; RSPV= right superior pulmonary vein.

Conclusion

MSCT has been demonstrated to allow non-invasive coronary angiography. To improve this imaging modality technique, optimization of patient preparation, data acquisition and reconstruction is required. Standardized data analysis and reporting is also needed. Several issues that are important related to these issues are summarized in this article.

When the currently available data are pooled, a high sensitivity with an excellent specificity is obtained. In particular, the specificity of 96% is an indicator that MSCT can adequately rule out coronary artery disease. It is important to keep in mind that this technique visualizes atherosclerosis and not ischemia. Therefore, the technique can not be compared directly with the currently available imaging modalities to non-invasively assess coronary artery disease, such as nuclear myocardial perfusion imaging and stress echocardiography. Rather, these techniques visualize the consequences of atherosclerosis and indicate whether ischemia is present or not. The precise role of these imaging modalities (MSCT to assess atherosclerosis and myocardial perfusion imaging or stress echocardiography to assess ischemia) is to be established. A potential scenario could be to use these techniques mainly in patients with an intermediate likelihood of coronary artery disease in a sequential manner. MSCT could first be applied to rule out coronary artery disease; if present, myocardial perfusion imaging could be used to refine the consequences of the atherosclerosis: ischemia or not.

References

1. Achenbach S, Giesler T, Ropers D, Ulzheimer S, Derlien H, Schulte C, Wenkel E, Moshage W, Bautz W, Daniel WG, Kalender WA, Baum U. Detection of coronary artery stenoses by contrast-enhanced, retrospectively electrocardiographically-gated, multi-slice spiral computed tomography. *Circulation*. 2001;103:2535-2538.
2. Nieman K, Oudkerk M, Rensing BJ, van Ooijen P, Munne A, van Geuns RJ, de Feyter PJ. Coronary angiography with multi-slice computed tomography. *Lancet*. 2001;357:599-603.
3. Schuijf JD, Bax JJ, Shaw LJ, de Roos A, Lamb HJ, van der Wall EE, Wijns W. Meta-analysis of comparative diagnostic performance of magnetic resonance imaging and multi-slice computed tomography for noninvasive coronary angiography. *Am Heart J*. 2006;151:404-411.
4. Cademartiri F, Mollet NR, Runza G, Baks T, Midiri M, McFadden EP, Flohr TG, Ohnesorge B, de Feyter PJ, Krestin GP. Improving diagnostic accuracy of MDCT coronary angiography in patients with mild heart rhythm irregularities using ECG editing. *AJR Am J Roentgenol*. 2006;186:634-638.
5. Cademartiri F, van der LA, Luccichenti G, Pavone P, Krestin GP. Parameters affecting bolus geometry in CTA: a review. *J Comput Assist Tomogr*. 2002;26:598-607.
6. Cademartiri F, Mollet N, van der LA, Nieman K, Pattynama PM, de Feyter PJ, Krestin GP. Non-invasive 16-row multi-slice CT coronary angiography: usefulness of saline chaser. *Eur Radiol*. 2004;14:178-183.
7. Cademartiri F, Luccichenti G, Marano R, Gualerzi M, Brambilla L, Coruzzi P. Comparison of monophasic vs biphasic administration of contrast material in non-invasive coronary angiography using a 16-row multi-slice Computed Tomography. *Radiol Med (Torino)*. 2004;107:489-496.
8. Cademartiri F, Nieman K, van der LA, Raaijmakers RH, Mollet N, Pattynama PM, de Feyter PJ, Krestin GP. Intravenous contrast material administration at 16-detector row helical CT coronary angiography: test bolus versus bolus-tracking technique. *Radiology*. 2004;233:817-823.
9. Jakobs TF, Becker CR, Ohnesorge B, Flohr T, Suess C, Schoepf UJ, Reiser MF. Multi-slice helical CT of the heart with retrospective ECG gating: reduction of radiation exposure by ECG-controlled tube current modulation. *Eur Radiol*. 2002;12:1081-1086.
10. Cademartiri F, Luccichenti G, Marano R, Nieman K, Mollet N, de Feyter P, Krestin GP, Pavone P, Bonomo L. Non-invasive angiography of the coronary arteries with multi-slice computed tomography: state of the art and future prospects. *Radiol Med (Torino)*. 2003;106:284-296.
11. Sato Y, Matsumoto N, Kato M, Inoue F, Horie T, Kusama J, Yoshimura A, Imazeki T, Fukui T, Furuhashi S, Takahashi M, Kanmatsuse K. Noninvasive assessment of coronary artery disease by multi-slice spiral computed tomography using a new retrospectively ECG-gated image reconstruction technique. *Circ J*. 2003;67:401-405.
12. Mollet NR, Cademartiri F, Nieman K, Saia F, Lemos PA, McFadden EP, Pattynama PM, Serruys PW, Krestin GP, de Feyter PJ. Multi-slice spiral computed tomography coronary angiography in patients with stable angina pectoris. *J Am Coll Cardiol*. 2004;43:2265-2270.
13. Nieman K, Cademartiri F, Lemos PA, Raaijmakers R, Pattynama PM, de Feyter PJ. Reliable noninvasive coronary angiography with fast submillimeter multi-slice spiral computed tomography. *Circulation*. 2002;106:2051-2054.
14. Ropers D, Baum U, Pohle K, Anders K, Ulzheimer S, Ohnesorge B, Schlundt C, Bautz W, Daniel WG, Achenbach S. Detection of coronary artery stenoses with thin-slice multi-detector row spiral computed tomography and multiplanar reconstruction. *Circulation*. 2003;107:664-666.
15. Austen WG, Edwards JE, Frye RL, Gensini GG, Gott VL, Griffith LS, McGoon DC, Murphy ML, Roe BB. A reporting system on patients evaluated for coronary artery disease. Report of the Ad Hoc Committee for Grading of Coronary Artery Disease, Council on Cardiovascular Surgery, American Heart Association. *Circulation*. 1975;51:5-40.
16. Schuijf JD, Bax JJ, Shaw LJ, de Roos A, Lamb HJ, van der Wall EE, Wijns W. Meta-analysis of comparative diagnostic performance of magnetic resonance imaging and multi-slice computed tomography for noninvasive coronary angiography. *Am Heart J*. 2006;151:404-411.
17. Ko YG, Choi DH, Jang YS, Chung NS, Shim WH, Cho SY, Yoo KJ, Chang BC, Choi BW. Assessment of coronary artery bypass graft patency by multi-slice computed tomography. *Yonsei Med J*. 2003;44:438-444.
18. Marano R, Storto ML, Maddestra N, Bonomo L. Non-invasive assessment of coronary artery bypass graft with retrospectively ECG-gated four-row multi-detector spiral computed tomography. *Eur Radiol*. 2004;14:1353-1362.

19. Nieman K, Pattynama PM, Rensing BJ, van Geuns RJ, de Feyter PJ. Evaluation of patients after coronary artery bypass surgery: CT angiographic assessment of grafts and coronary arteries. *Radiology*. 2003;229:749-756.
20. Ropers D, Ulzheimer S, Wenkel E, Baum U, Giesler T, Derlien H, Moshage W, Bautz WA, Daniel WG, Kalender WA, Achenbach S. Investigation of aortocoronary artery bypass grafts by multi-slice spiral computed tomography with electrocardiographic-gated image reconstruction. *Am J Cardiol*. 2001;88:792-795.
21. Willmann JK, Weishaupt D, Kobza R, Verdun FR, Seifert B, Marincek B, Boehm T. Coronary artery bypass grafts: ECG-gated multi-detector row CT angiography--influence of image reconstruction interval on graft visibility. *Radiology*. 2004;232:568-577.
22. Yoo KJ, Choi D, Choi BW, Lim SH, Chang BC. The comparison of the graft patency after coronary artery bypass grafting using coronary angiography and multi-slice computed tomography. *Eur J Cardiothorac Surg*. 2003;24:86-91.
23. Martuscelli E, Romagnoli A, D'Eliseo A, Tomassini M, Razzini C, Sperandio M, Simonetti G, Romeo F, Mehta JL. Evaluation of venous and arterial conduit patency by 16-slice spiral computed tomography. *Circulation*. 2004;110:3234-3238.
24. Salm LP, Bax JJ, Jukema JW, Schuijf JD, Vliegen HW, Lamb HJ, van der Wall EE, de Roos A. Comprehensive assessment of patients after coronary artery bypass grafting by 16-detector-row computed tomography. *Am Heart J*. 2005;150:775-781.
25. Schuijf JD, Bax JJ, Jukema JW, Lamb HJ, Warda HM, Vliegen HW, de Roos A, van der Wall EE. Feasibility of assessment of coronary stent patency using 16-slice computed tomography. *Am J Cardiol*. 2004;94:427-430.
26. Dirksen MS, Bax JJ, de Roos A, Jukema JW, van der Geest RJ, Geleijns K, Boersma E, van der Wall EE, Lamb HJ. Usefulness of dynamic multi-slice computed tomography of left ventricular function in unstable angina pectoris and comparison with echocardiography. *Am J Cardiol*. 2002;90:1157-1160.
27. Schuijf JD, Bax JJ, Salm LP, Jukema JW, Lamb HJ, van der Wall EE, de Roos A. Noninvasive coronary imaging and assessment of left ventricular function using 16-slice computed tomography. *Am J Cardiol*. 2005;95:571-574.
28. Grude M, Juergens KU, Wichter T, Paul M, Fallenberg EM, Muller JG, Heindel W, Breithardt G, Fischbach R. Evaluation of global left ventricular myocardial function with electrocardiogram-gated multidetector computed tomography: comparison with magnetic resonance imaging. *Invest Radiol*. 2003;38:653-661.
29. Juergens KU, Grude M, Maintz D, Fallenberg EM, Wichter T, Heindel W, Fischbach R. Multi-detector row CT of left ventricular function with dedicated analysis software versus MR imaging: initial experience. *Radiology*. 2004;230:403-410.
30. Mahnken AH, Spuentrup E, Niethammer M, Buecker A, Boese J, Wildberger JE, Flohr T, Sinha AM, Krombach GA, Gunther RW. Quantitative and qualitative assessment of left ventricular volume with ECG-gated multi-slice spiral CT: value of different image reconstruction algorithms in comparison to MRI. *Acta Radiol*. 2003;44:604-611.
31. Schuijf JD, Bax JJ, Jukema JW, Lamb HJ, Vliegen HW, Salm LP, de Roos A, van der Wall EE. Noninvasive angiography and assessment of left ventricular function using multi-slice computed tomography in patients with type 2 diabetes. *Diabetes Care*. 2004;27:2905-2910.
32. Haissaguerre M, Jais P, Shah DC, Takahashi A, Hocini M, Quiniou G, Garrigue S, Le Mouroux A, Le Metayer P, Clementy J. Spontaneous initiation of atrial fibrillation by ectopic beats originating in the pulmonary veins. *N Engl J Med*. 1998;339:659-666.
33. Ho SY, Cabrera JA, Tran VH, Farre J, Anderson RH, Sanchez-Quintana D. Architecture of the pulmonary veins: relevance to radiofrequency ablation. *Heart*. 2001;86:265-270.
34. Jongbloed MR, Dirksen MS, Bax JJ, Boersma E, Geleijns K, Lamb HJ, Van Der Wall EE, de Roos A, Schalij MJ. Atrial fibrillation: multi-detector row CT of pulmonary vein anatomy prior to radiofrequency catheter ablation--initial experience. *Radiology*. 2005;234:702-709.
35. Jongbloed MR, Bax JJ, Lamb HJ, Dirksen MS, Zeppenfeld K, Van Der Wall EE, de Roos A, Schalij MJ. Multislice computed tomography versus intracardiac echocardiography to evaluate the pulmonary veins before radiofrequency catheter ablation of atrial fibrillation: a head-to-head comparison. *J Am Coll Cardiol*. 2005;45:343-350.